

Supplementary Information

Catalytic impact of alloyed Al on the corrosion behavior of Co₅₀Ni₂₃Ga₂₆Al_{1.0} magnetic shape memory alloy and catalysis applications for efficient electrochemical H₂ generation

Mohammed. A. Amin*^{1,2}, Nader El-Bagoury^{1,3}, M. H. H. Mahmoud^{1,3}, M.M. Hessien^{1,3},

Sayed S. Abd El-Rehim², Joanna Wysocka⁴, Jacek Ryl⁴

¹Department of Chemistry, Faculty of Science, Taif University, Saudi Arabia

²Department of Chemistry, Faculty of Science, Ain Shams University, 11566 Abbassia, Cairo, Egypt

³Central Metallurgical Research and Development Institute (CMRDI), P.O. Box: 87 Helwan , Cairo,
Egypt

⁴Department of Electrochemistry, Corrosion and Materials Engineering, Chemical Faculty, Gdańsk
University of Technology, Narutowicza 11/12, 80-233 Gdańsk. Poland

1. Conversion of the working electrode's potential from the SCE scale to the RHE scale

In this work, the potentials were measured with respect to SCE (E_{SCE} or $E_{\text{electrode}}$) and are reported vs reversible hydrogen electrode (RHE), E_{RHE} . Conversion to RHE was done using the relation [1]:

$$E_{\text{RHE}} = E_{\text{SCE}} - E^{\circ}_{\text{H}_2/2\text{H}^+} + 0.244 \quad (1)$$

where $E^{\circ}_{\text{H}_2/2\text{H}^+}$ is the reversible hydrogen potential, given by Nernst equation ($E^{\circ}_{\text{H}_2/2\text{H}^+} = -0.059 \text{ pH}$); a pH value of ~ 13 was measured for the test solution (0.1 M KOH). The number +0.244 in Eq. (1) denotes the standard potential (in Volts) of the used SCE {Cl⁻ (4M) | Hg₂Cl_{2(s)} | Hg(l) | Pt @ 25 °C}. For instance, for $E_{\text{electrode}} = -2 \text{ V(SCE)}$, $E_{\text{HER}} = (-2) - (-0.059 \times 13) + 0.244 = -0.989 \text{ V(RHE)}$.

2. Faradaic efficiency measurements

Measurements were conducted in a custom-made airtight electrolysis cell containing a 0.1 M KOH solution by holding the electrode at -0.8 V vs RHE for 1 h. Gas chromatography was conducted on an Agilent 7890A gas chromatograph with a pneumatically operated automatic gas sampling valve to monitor the evolved H₂ gas. The electrolysis cell was connected to the gas chromatography system via bespoke airtight glass-to-metal adapters and copper tubing with an internal diameter of 1/8 in. The oven temperature was set to 45 °C, and the carrier gas was Ar with a flow rate of approximately 3 mL min⁻¹.

3. Effect of Al addition on the uniform corrosion rate of CoNiGa SMA

3.1. Tafel polarization and LPR measurements

Figures S1 and S2 show respectively the cathodic and anodic polarization curves and LPR plots for alloys I and II in 0.5 M NaCl solution at 25 °C.

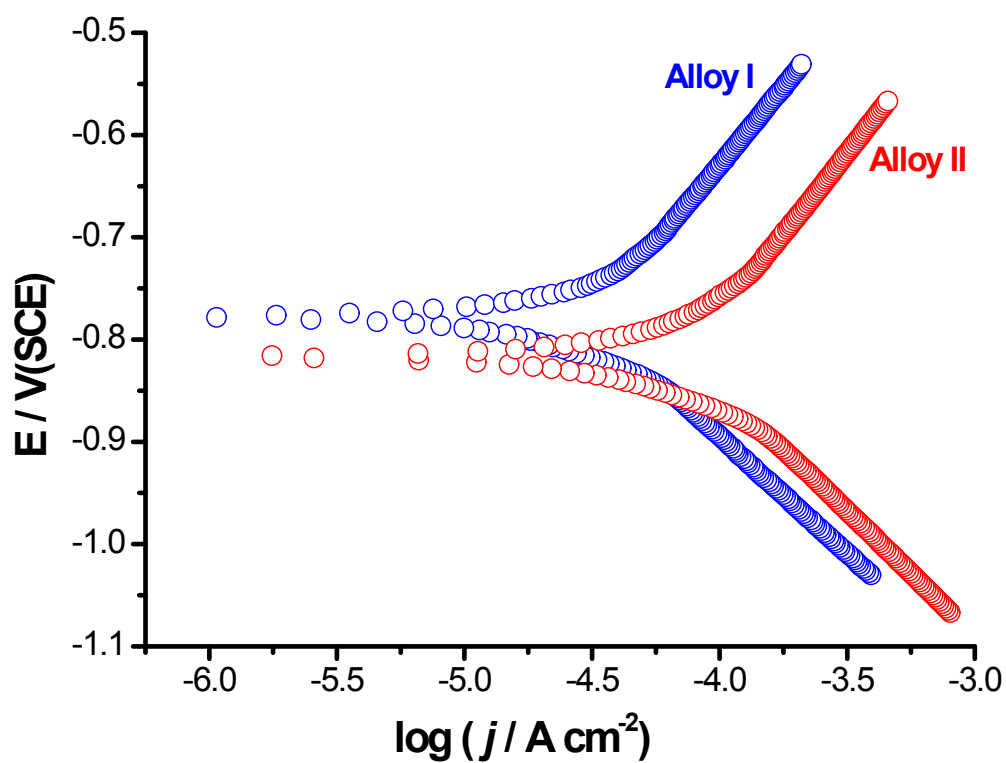


Figure S1 - Cathodic and anodic polarization curves recorded for alloys I (CoNiGa) and II (CoNiGaAl) in 0.5 M NaCl solutions at a scan rate of 1.0 mV s^{-1} at $25 \text{ }^\circ\text{C}$.

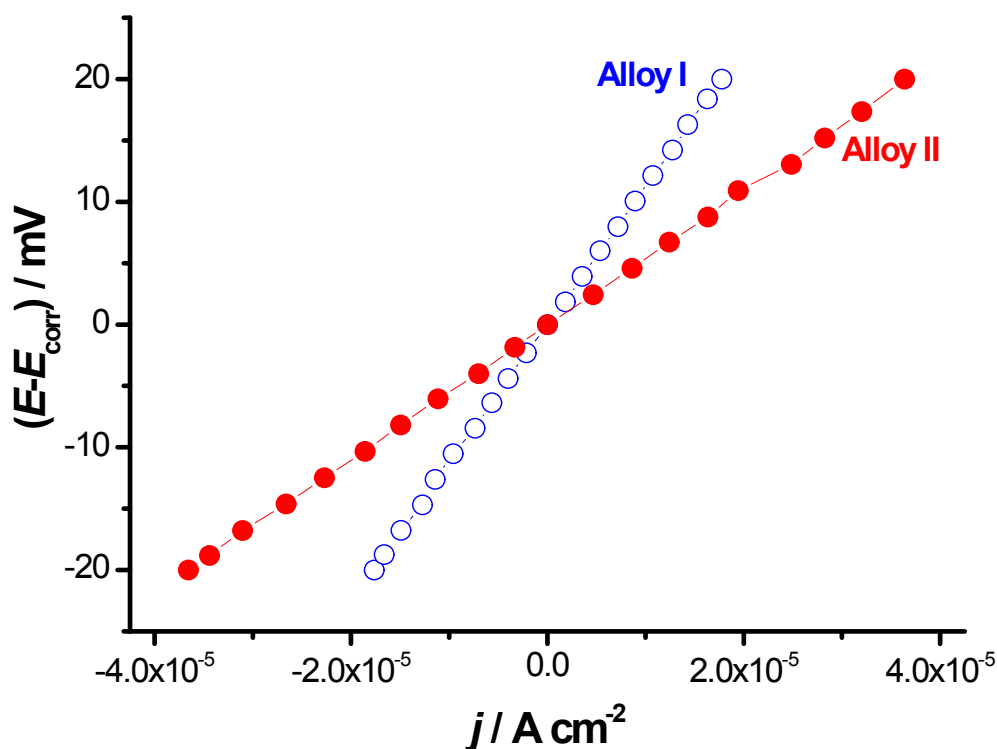


Figure S2 - Plots of linear polarization resistance (LPR) measurements recorded for alloys I (CoNiGa) and II (CoNiGaAl) in 0.5 M NaCl solutions at a scan rate of 0.167 mV s⁻¹ at 25 °C.

The various electrochemical corrosion parameters derived from such polarization measurements are presented in Table S1. Such parameters were calculated on the basis of potentiodynamic potential-current characteristics in the Tafel potential region ($E = E_{\text{corr}} \pm 250$ mV) Fig. S1, and in the vicinity of the corrosion potential ($E = E_{\text{corr}} \pm 20$ mV), Fig. S2. It follows from Fig. S1 that alloy II (the CoNiGa SMA alloyed with Al) exhibited lower anodic and cathodic overpotentials (and hence higher rates of corrosion) than alloy I (the Al-free SMA). This is obvious from the data of Table 2, which showed that alloy II recorded a j_{corr} value of 0.08 mA cm⁻², employing Tafel extrapolation method, which is 2.4 times greater than that recorded for alloy I (0.033 mA cm⁻²). These findings reveal that the uniform corrosion rate enhances when our tested CoNiGa SMA (alloy I) is alloyed with Al (alloy II here), demonstrating the accelerating (activation) influence of alloyed Al.

Table S1 – Mean value (standard deviation) of the various electrochemical parameters obtained from Tafel extrapolation and linear polarization resistance methods performed for alloys I and II in 0.5 M NaCl solutions at 25 °C.

Tested alloy	Tafel extrapolation method				LPR method	
	$-E_{\text{corr}} /$ mV(SCE)	$-\beta_c /$ mV dec ⁻¹	$\beta_a /$ mV dec ⁻¹	$j_{\text{corr}} /$ mA cm ⁻²	$R_p /$ Ω cm ²	$j_{\text{corr}} /$ mA cm ⁻²
Alloy I	-780	-230	310	0.033	1509	0.038
Alloy II	-820	-240	313	0.08	656	0.09

Values of the anodic and cathodic Tafel slopes (β_a and β_c) obtained from the analysis of the Tafel plots (Fig. S1 and Table S1) and those of the polarization resistance, $R_p = (dE/dj)_{E=E_{\text{corr}}}$ [1], obtained from the slopes of the LPR plots, Fig. S2, are introduced in Stern-Geary equation [2] to get accurate values for j_{corr} , Table S1.

$$j_{\text{corr}} = B/R_p = \{\beta_a \beta_c / 2.303(\beta_a + \beta_c)\} / R_p \quad (1)$$

Obviously, a good agreement exists between the values of j_{corr} evaluated from the Tafel extrapolation method and those calculated from the LPR method. As clearly seen in Table S1, alloy I recorded an R_p value of 1509 Ω cm², which is 2.3 times greater than that measured for alloy II (656 Ω cm²). Generally, the increase in the R_p value suggests that the corrosion rate is decreased, corresponding to improved corrosion resistance. Thus LPR measurements go parallel with Tafel extrapolation method revealing the lower corrosion resistance of alloy II as compared with alloy I. To gain more insight on the activation influence of alloyed Al towards passivity of our tested CoNiGa SMA, impedance measurements were performed for alloy I and II in 0.5 M NaCl solutions at the respective E_{corr} , Fig. S3.

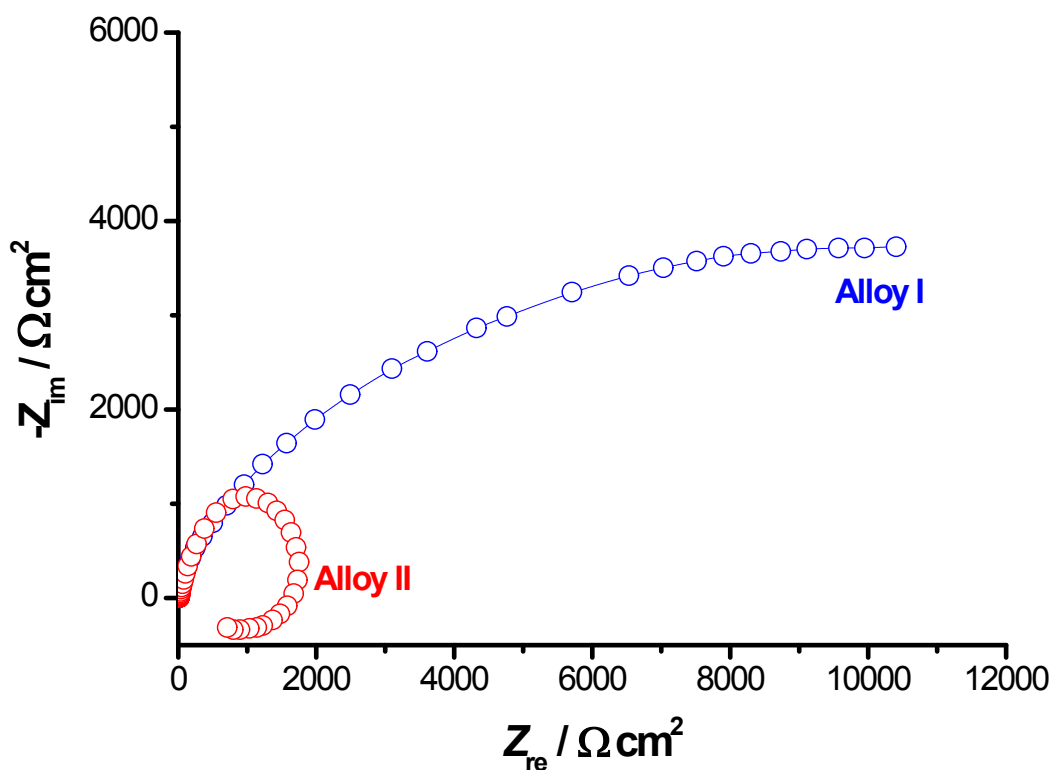


Figure S3 – Complex-plane impedance plots recorded for alloys I (CoNiGa) and II (CoNiGaAl) in 0.5 M NaCl solutions at the respective E_{corr} at 25 °C.

It can be seen that alloy I recorded a high charge-transfer resistance value of 1880 $\Omega \text{ cm}^2$, which is 3 times larger than that of alloy II (615 $\Omega \text{ cm}^2$). These findings go parallel with polarization studies supporting the low corrosion resistance of alloy II as compared with alloy I. The significantly reduced impedance of alloy II, as a result of alloyed Al which weakens the passive layer, as compared with alloy I afforded markedly faster corrosion kinetics (i.e., enhanced the electron transfer) on its surface than on the surface of alloy I.

The results of ICP-AES measurements, Table S2, came to the same conclusion and revealed that the concentrations of both Ni^{2+} and Co^{2+} ions, released in solution due to corrosion, increase with time. Their values are always higher for alloy II than alloy I at any given time, thus confirming polarization and impedance studies. SEM examinations, Fig. S4, also confirmed the above findings, revealing the extremely high corrosion susceptibility of alloy II (image (b)) in a comparison with alloy I, image (a).

Table S2 – Concentrations of Ni²⁺ and Co²⁺ ions, determined from ICP-AES method of chemical analysis, released from the tested alloy in the corrosive medium (0.5 M NaCl) at 25 °C as a function of the immersion time periods (1-15 days).

Time / days	Alloy I		Alloy II	
	[Co ²⁺] / ppm	[Ni ²⁺] / ppm	[Co ²⁺] / ppm	[Ni ²⁺] / ppm
1	Nil	Nil	0.29	0.05
3	0.16	Nil	0.68	0.26
12	1.36	0.51	1.74	0.73
15	1.96	0.8	2.53	1.26

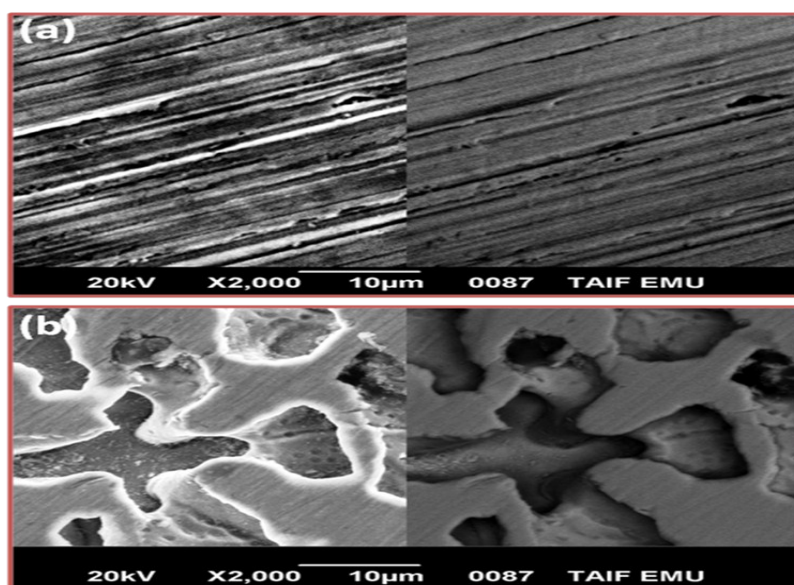


Figure S4 – SEM images pictured for alloys I (image (a)) and II (image (b)) after 24 hours of immersion in 0.5 M NaCl solution at 25 °C.

4. Effect of applied anodic potential on the current/time responses of the tested MSMA

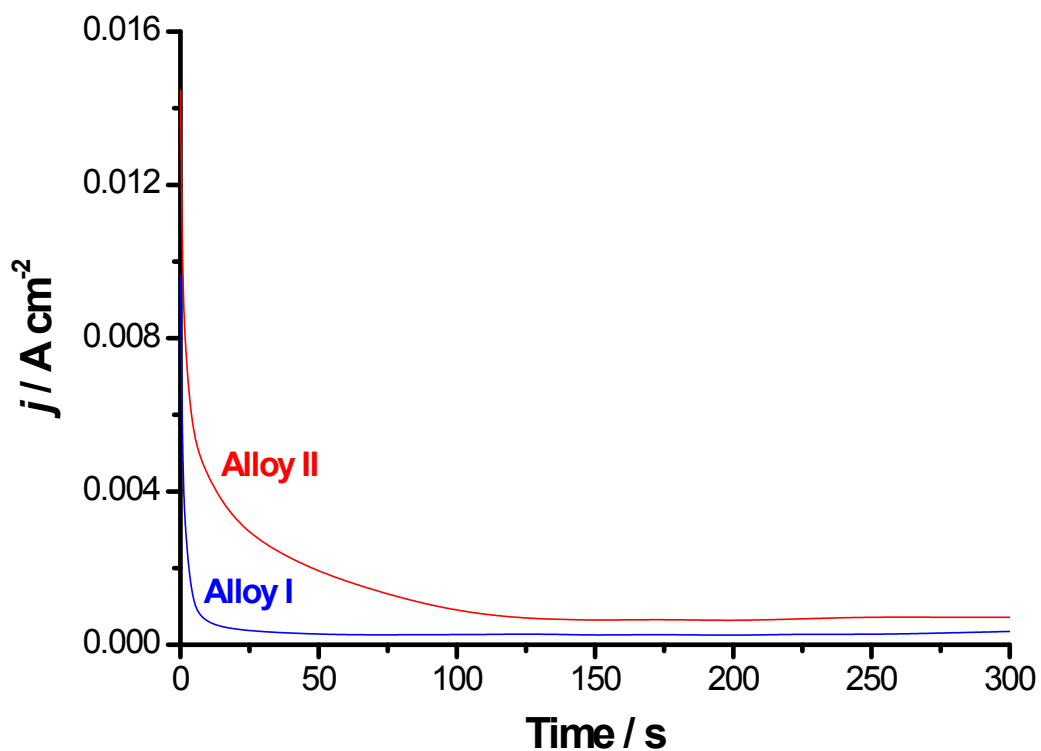


Figure S5 – Chronoamperometry measurements recorded for alloys I (CoNiGa SMA) and II (CoNiGaAl SMA) in 0.5 M NaCl solutions at $E_a = -0.2$ V(SCE) at 25 °C.

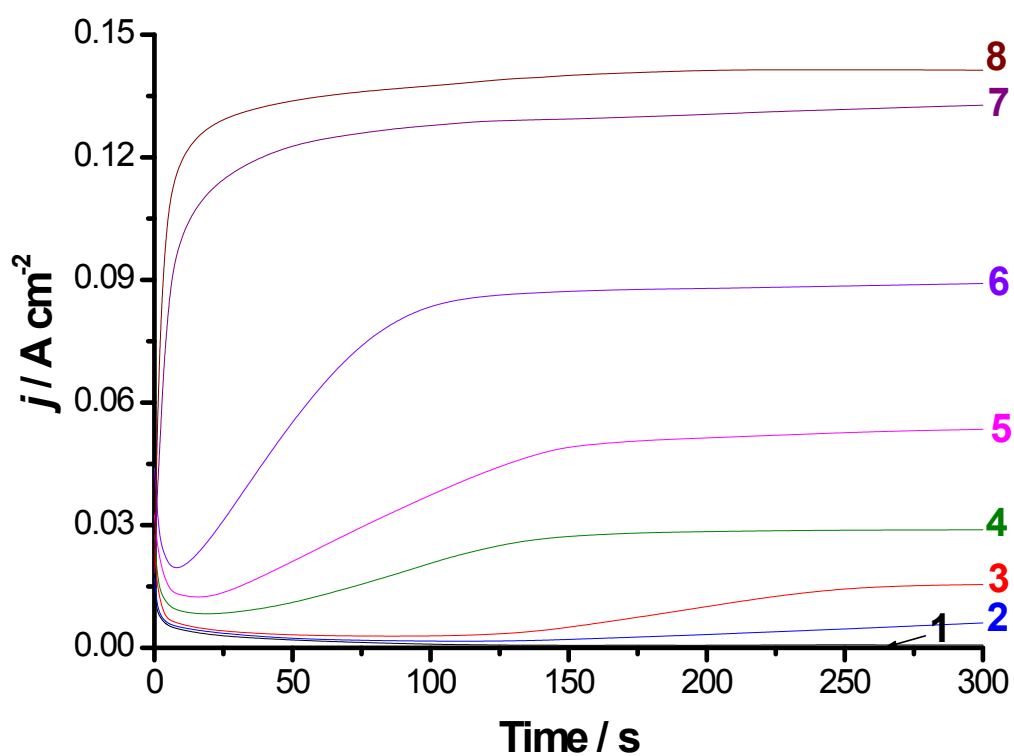


Figure S6 – Chronoamperometry measurements recorded for alloy II (CoNiGaAl SMA) in 0.5 M NaCl solutions at 25 °C as a function of the applied anodic potential (E_a). **(1)** -0.2 V(SCE); **(2)** -0.1 V(SCE); **(3)** 0.0 V(SCE); **(4)** +0.1 V(SCE); **(5)** +0.2 V(SCE); **(6)** +0.3 V(SCE); **(7)** +0.4 V(SCE); **(8)** +0.5 V(SCE).

5. Determination of the Exchange Current Density, j_0

The Tafel equation $\{\eta = (2.3RT/naF) \log j_0 - (2.3RT/naF) \log j\}$ is the high overpotential limiting case of the Butler-Volmer equation. The most important Tafel parameters are the cathodic Tafel slope (β_c) and the exchange current density (j_0). The linear scan voltammogram generated during the HER measurements (Fig. 3(a) in the main text) are re-plotted in the form of the overpotential, η , vs. $\log j$. The resulting graph is known as a Tafel plot, Fig. S7 is a representative example, and Tafel parameters can be determined by fitting the linear portion of the plot, as shown below.

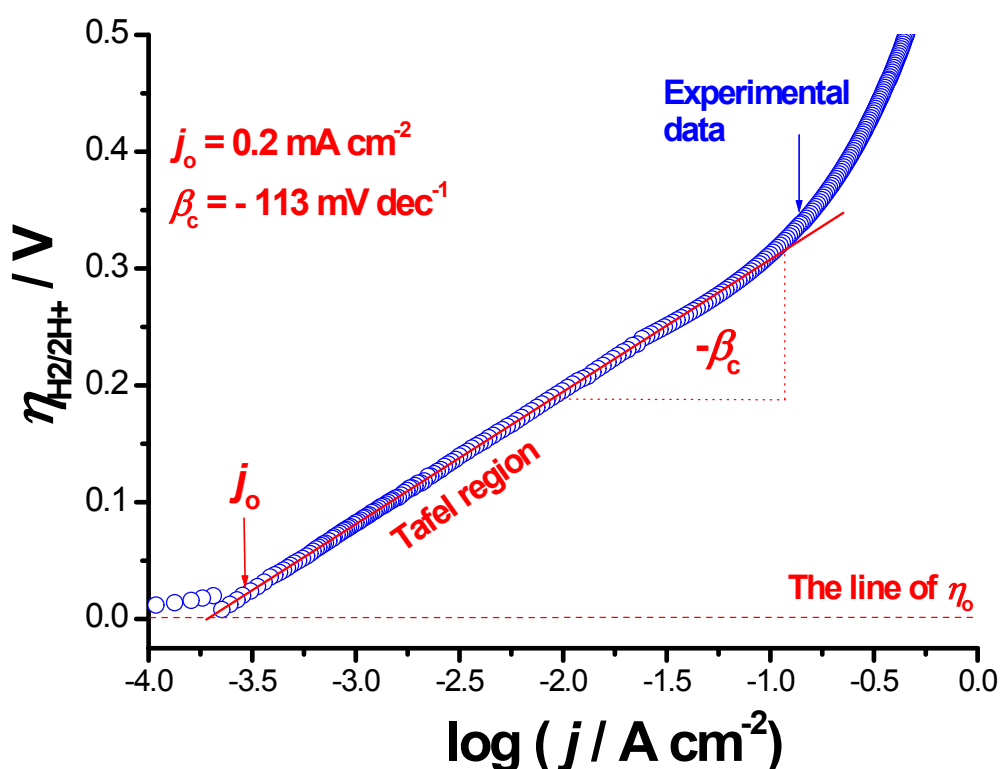
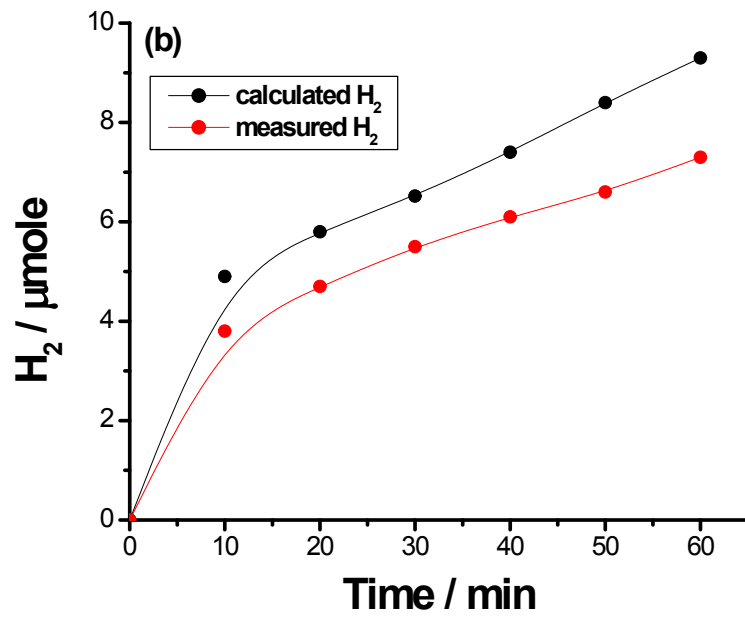
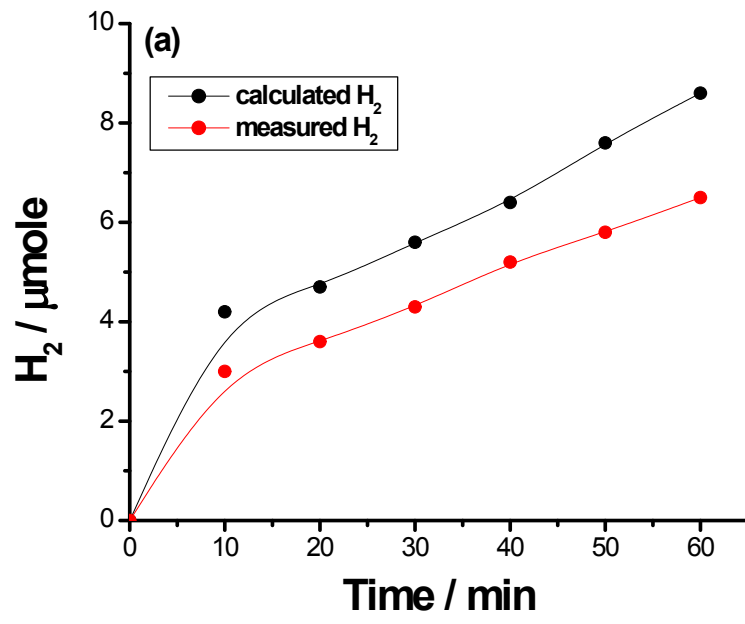


Figure S7: Tafel equation fitting (the red solid line) to the experimental cathodic polarization data recorded for alloy II after 24h of immersion in 0.5 M NaCl solution at 25 °C. Measurements were conducted in 0.1 M KOH solution at a scan rate of 5.0 mV s⁻¹ at 25 °C.

Table S3 – Mean values of the roughness factor (R_f) obtained from EIS technique for the studied catalysts. Measurements were conducted in 0.1 M KOH solutions at cathodic potentials -0.3, -0.5, and -0.7 V vs SCE at 25 °C. The theoretical (calculated) value of Q equals $20 S^n (\omega^{-1} \text{ cm}^{-2})^{3,4}$.

Catalyst	$E /$ V (RHE)	$Q_{\text{measured}} =$ $(Q_1 + Q_2)^*$	$R_f =$ $Q_{\text{measured}} / Q_{\text{calculated}}$
Co	-0.3	41.1	2.06
	-0.5	56.3	2.82
	-0.7	71.2	3.56
Ni	-0.3	50.5	2.53
	-0.5	71.1	3.56
	-0.7	92	4.6
Co ₅₀ Ni ₅₀	-0.3	81.5	4.08
	-0.5	107.9	5.4
	-0.7	145.6	7.28
Alloy I (without corrosion pretreatment)	-0.3	97.1	4.86
	-0.5	148	7.4
	-0.7	199.4	9.97
Alloy I (after corrosion pretreatment)	-0.3	118.9	5.95
	-0.5	167.2	8.36
	-0.7	236.6	11.83
Alloy II (without corrosion pretreatment)	-0.3	160.3	8.02
	-0.5	282.4	14.12
	-0.7	387	19.35
Alloy II (after corrosion pretreatment)	-0.3	312	15.6
	-0.5	558.7	27.94
	-0.7	1180.7	59.04

*values of Q_1 and Q_2 were taken from Table 2 in the main manuscript.



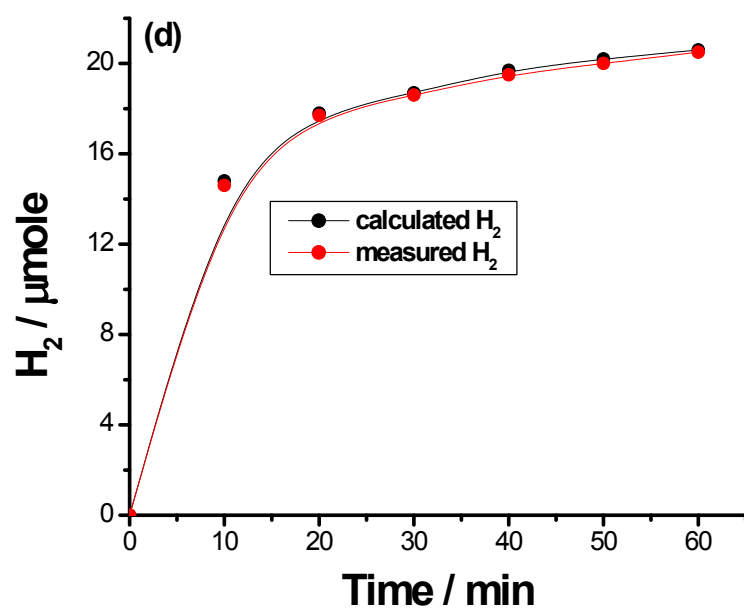
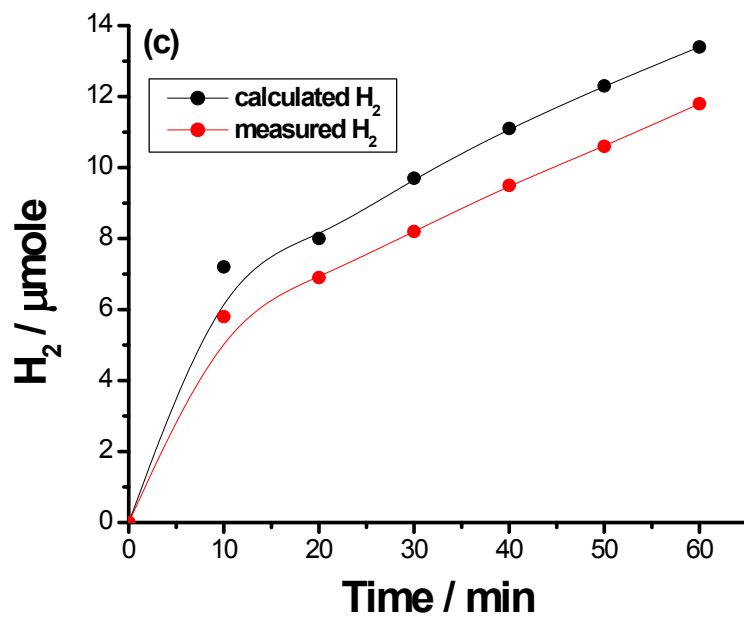


Figure S8: Volume of H₂ calculated from the amount of charge passed (assuming 100% Faradaic efficiency) and that of H₂ measured from gas chromatography during 1 h of a controlled potential electrolysis run (the working electrode is held at -0.8 V vs RHE in 0.1 M KOH for 1h) of the studied catalysts. **(a)** alloy I without corrosion pretreatment; **(b)** alloy I with corrosion pretreatment; **(c)** alloy II without corrosion pretreatment; **(d)** Pt/C.

Table S4 - Chemical composition of γ and martensite phases in both investigated alloys.

Alloy	Martensite phase (at%)				γ phase (at%)				Vol. % of γ phase
	Co	Ni	Ga	Al	Co	Ni	Ga	Al	
0% Al	44.93	25.30	29.76		57.69	22.90	19.41		42.56
		0.00				0.00			
1% Al	44.02	25.59	29.48		57.85	22.00	19.46		37.44
		0.90				0.69			

References

1. F. Mansfeld, *Corrosion*, 1981, **37**, 301.
2. M. Stern and A. L. Geary, *J. Electrochem. Soc.*, 1957, **104**, 56.
3. B. Losiewicz, A. Budniok, E. Rowinski, E. Lagiewka and A. Lasia, *Int. J. Hydrogen Energ*, 2004, **29**, 145.
4. C. González-Buch, I. Herraiz-Cardona, E.M. Ortega, J. García-Antón and V. Pérez-Herranz, *Chem. Eng. Trans.*, 2013, **32**, 865-870.